JOURNAL OF MATERIALS SCIENCE 31 (1996) 3043–3050

Quantitative measurement of roughness of fractured rubber surfaces by an image processing technique

L. GANESAN, PRITIMOY BHATTACHARYYA, ANIL K. BHOWMICK*‡
*Dept. of Computer Science and Engineering and *Rubber Technology Center, Indian Institute of Technology, Kharagpur-721302, India*

In this paper, an image processing technique has been employed to quantitatively analyse various fractured surfaces of rubber and measure roughness. The image surfaces are represented in terms of a closed set of orthogonal polynomials. The significant orthogonal effects are measured and combined to represent the local texture, called pronum. The frequency of occurrence of the pronums is the prospectrum, a global descriptor. A few statistical parameters have been calculated from the prospectrum and correlated to the roughness of the fractured surfaces. Using the image processing technique, the laborious procedure involved in quantification, especially of irregular microfeatures, has been shown to be overcome.

1. Introduction

Fracture of rubber generates typical surfaces, which provide information on deformation, crack initiation, crack deviation, crack propagation, etc. In earlier studies, the morphology of a large number of fracture surfaces has been reported [1–14]. These describe mechanism of fracture of rubber under a variety of conditions. For example, Thomas and Greensmith [1–3] discussed rough or irregular surface in natural rubber and styrene–butadiene rubber at low rates of crack growth with a transition to smoother appearances at higher velocities. Carbon-black-filled vulcanizates show tear tip deviation, branching of crack tip, etc., as compared to gum samples, showing smoother tear lines propagating from one end to another [4]. The abrasion patterns obtained with stronger and weaker rubbers are clearly distinguishable [6]. Bhowmick and coworkers revealed the mechanism of fracture of a few rubbers and thermoplastic elastomers from the micrographs [8–12]. Bhowmick and De summarized this information for rubber in a recent book [15]. Fractographic parameters, if properly quantified, should be related to the fracture energy. Hence, analysis of these surfaces gives valuable information to supplement theoretical studies along with additional insight into failure mechanisms.

Quantitative studies in these respects have been attempted in the past. For example, Schallamach correlated ridge spacing on the worn surface with shear modulus [6, 7]. Fukahori and Andrews [5] described surface roughness as a function of hysteresis in the rubber surrounding the propagating crack. Studies by Gent and Pulford on torn rubber surface are notable [16]. A quantitative correlation between the tensile strength and the distance between the tear lines and crack lines observed on the fracture surface of natural rubber has been put forward by Deuri and Bhowmick [17]. Thavamani and Bhowmick proposed a universal relationship between ridge spacing per unit frictional work and abradability [18].

However, the methods adopted by the previous workers are laborious. Also, when the surface morphology is not uniform, it is difficult to quantify. Recently, we have used an image processing technique to quantify worn surfaces of rubber with some statistical parameters. This method is quick and is able to analyse the non-uniform microfeatures on the fracture surface. The objective of the present study is to quantitatively measure the surface roughness of a tensile fractured surface by using an image processing technique as discussed below. These surfaces are shown to have a complicated nature and have been analysed with difficulty by the conventional technique. We have chosen photographs from two earlier papers on tensile rupture of rubber by Deuri and Bhowmick [17] and Fukahori and Andrews [5]. These are shown in Figs 1a–c and 2a–m.

2. Our method for texture analysis

A 2D image is a flat object whose brightness or colour may vary from point to point. This variation can be represented mathematically by a function of two variables x and y represented by a single real-valued function $f(x, y)$. The value of this function at a point will be called the gray level or brightness of the image at that point. Thus, a digital image can be regarded as an integer array. The elements of a digital image array are called picture elements, pixels, or pels. Texture

‡ Author to whom all correspondence should be addressed.

0022–2461

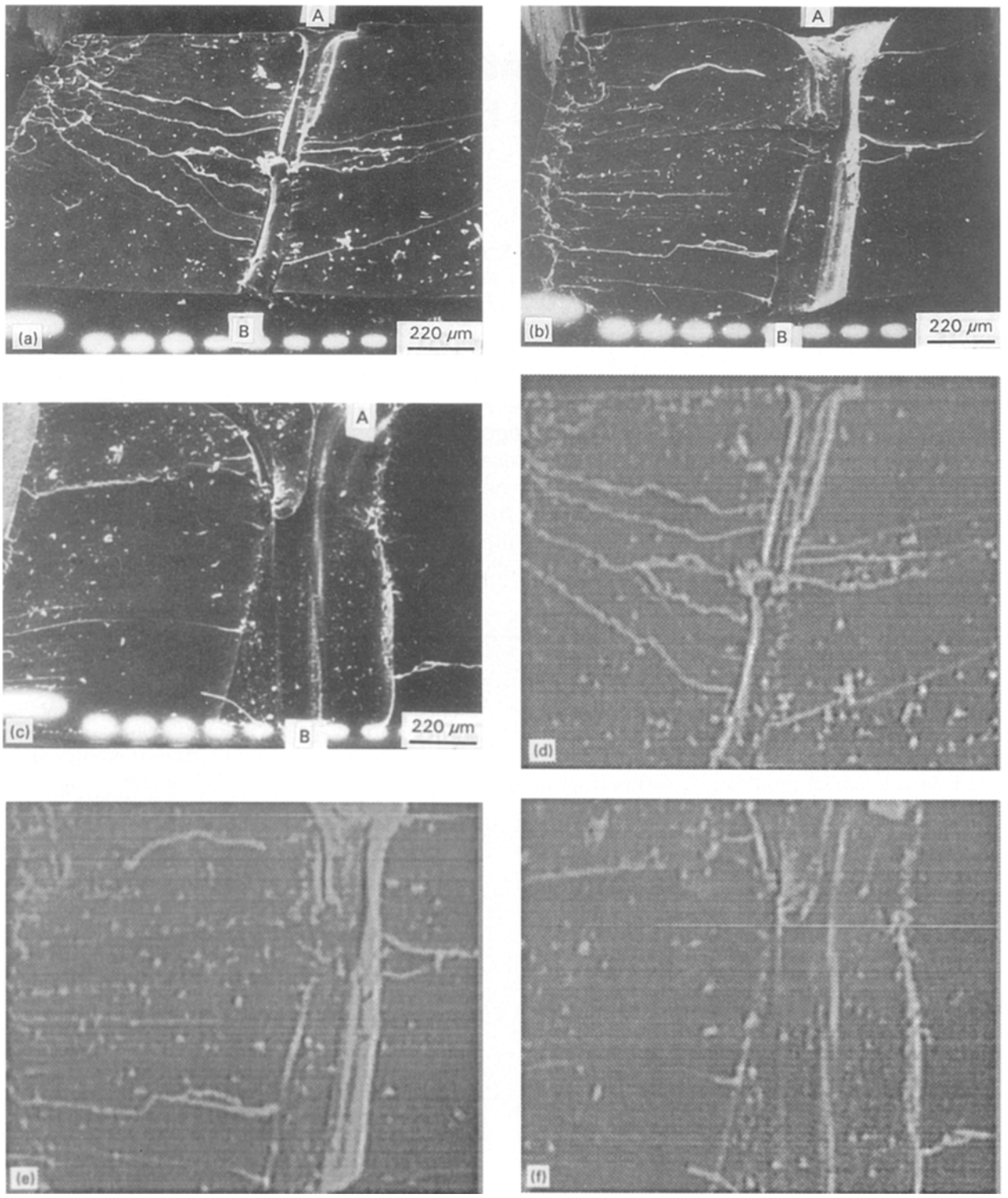

Figure 1 SEM photograph of tensile fractured surface for unaged NR gum vulcanizate (a) with precut of 0.49 mm; (b) at critical cut length; and (c) with precut of 1.49 mm. With kind permission from *J. Mater. Sci.*, Chapman & Hall. (d)–(f) Digitized versions of the images shown in (a)–(c), respectively.

could be defined as a structure composed of a large number of more or less ordered, similar elements or patterns. Textures are normally ranging from micro to macro. A micro texture appears only in a small area of digital image with very high gray level variations, i.e. significant tonal variation within a small image region. Micro textures can be studied effectively by using local properties. The quantified local properties of a micro texture are called the local descriptors for the texture or pronum. The whole textured image can be represented globally by computing the frequency of occurrences of pronums, which will be called the prospectrum. The prospectrum is unique for a textured image.

Consider an $(N*N)$ gray level image $f(x, y)$ where x, y are the two coordinates; $f(x, y)$ can be expressed as

$$f(x, y) = g(x, y) + \eta(x, y)$$

where $g(x, y)$ accounts for the variation due to cartesian coordinates in $f(x, y)$ and $\eta(x, y)$ is the additive noise. The variation $g(x, y)$ can be approximated by using an appropriate set of orthogonal functions in order to determine a closed set of orthogonal effects [19].

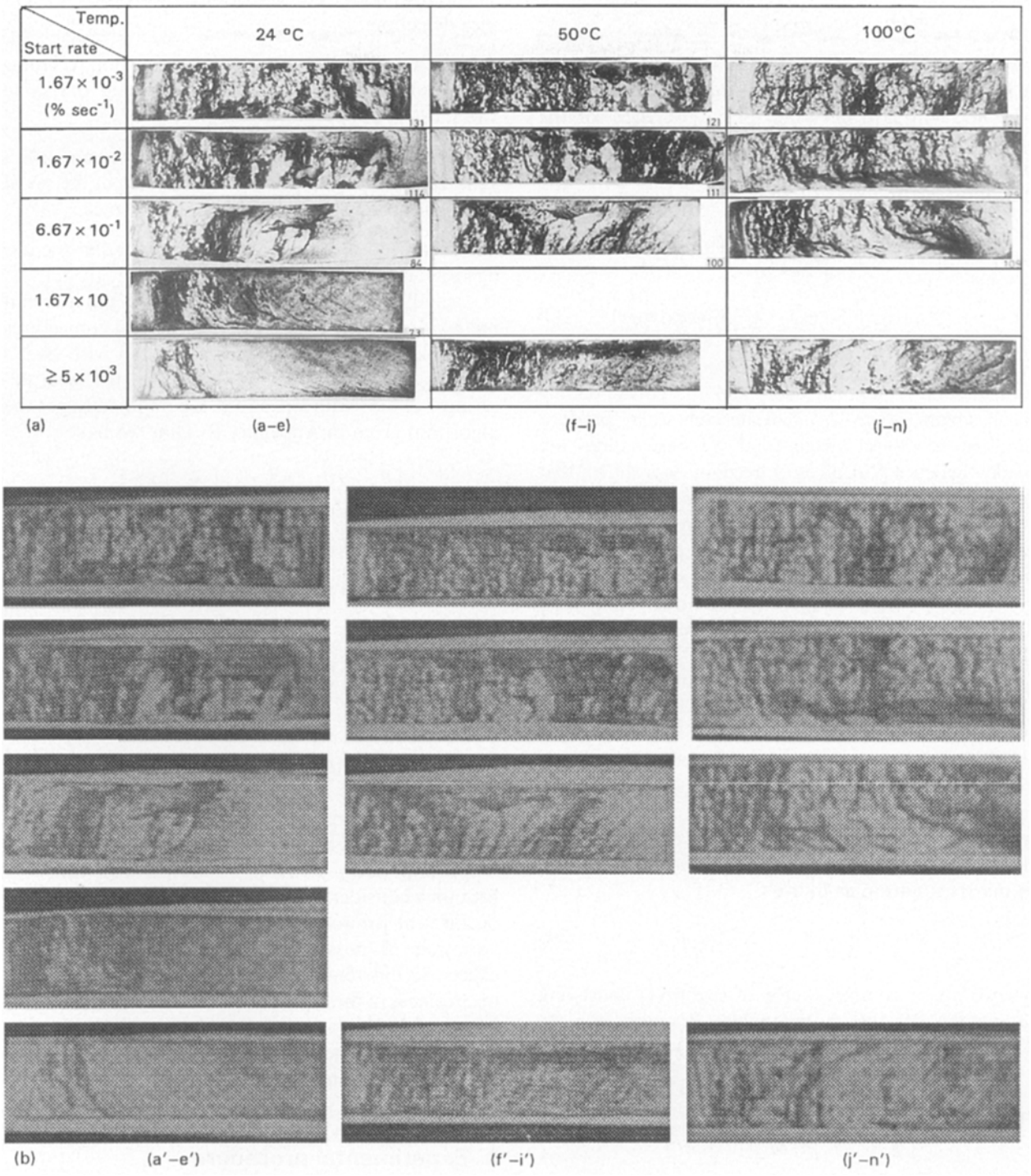

*Figure 2*a Fracture surfaces of SBR in notched specimens over the range of strain rates at 24 °C. (a–e), 50 °C (f–i) and 100 °C (j–m). Magnification 5 ×. With kind permission from *J. Mater. Sci.*, Chapman & Hall. Fig. 2b: (a)–(m) Digitized version of the images shown in (a)–(m), respectively.

In order to describe texture, let us assume that texture can be divided into K different classes, T_L, $L = 1,2,3, \ldots, K$, corresponding to primitives and their placements. Each of the classes can be characterized in terms of a closed set of orthogonal effects.

Let

$$\alpha = \{\alpha_{ij}(x, y), i, j = 0, 1, 2, \ldots, N - 1\}$$

be the N^2 linearly independent orthogonal functions forming the basis for computing the orthogonal effects of variation due to the cartesian coordinates. A suitable subset ψ_L of α is then chosen such that the subset of orthogonal effects will be sufficient to specify uniquely any texture element of a class T_L. In the absence of noise, the variation due to the cartesian coordinate in an image containing any member of a class T_L can be expressed as

$$g_L(x, y) = \sum_{\alpha_{ij} \in \psi_L} \sum \beta_{ij}\alpha_{ij}(x, y) \quad (1)$$

Hence, in the presence of noise, the gray level image $f(x, y)$ containing a member of a class T_L can be specified as

$$f(x, y) = \sum_{\alpha_{ij} \in \psi_L} \sum \beta_{ij}\alpha_{ij}(x, y) + \sum_{\alpha_{ij} \notin \psi_L} \sum \beta_{ij}\alpha_{ij}(x, y) \quad (2)$$

or

$$f(x, y) = \hat{g}(x, y) + \hat{\eta}(x, y)$$

where $\hat{g}$ and $\hat{\eta}$ are independent. The expected value of $\hat{g}$, $E(\hat{g}) = g$ and each β_{ij}:$\alpha_{ij} \notin \psi_L$ has an expected value of 0 and standard deviation of σ_η. Further, for the sake of computational simplicity, the orthogonal function α_{ij}'s are assumed to be separable. As a result, Equation 2 can be rewritten as

$$f(x, y) = \sum_{\alpha_{ij} \in \psi_L} \sum \beta_{ij}\phi_i(x)\phi_j(y) + \sum_{\alpha_{ij} \notin \psi_L} \sum \beta_{ij}\phi_i(x)\phi_j(y) \quad (3)$$

We call β_{ij} and $\beta_{ij}^2\langle\phi_i, \phi_i\rangle\langle\phi_j, \phi_j\rangle$ respectively the estimates of orthogonal effect and the corresponding mean square where $\langle\ \rangle$ indicates the scalar product. Since in an $(N*N)$ image, total N^2 observations are made, there are N degrees of freedom. It is shown that each of N^2 $\beta_{ij}^2\langle\phi_i, \phi_i\rangle\langle\phi_j, \phi_j\rangle/\sigma_\eta^2$ is a χ^2 variate with 1 degree of freedom. An estimate of error variance can be calculated by adding together $\beta_{ij}^2\langle\phi_i, \phi_i\rangle\langle\phi_j, \phi_j\rangle$: $\alpha_{ij} \notin \psi_L$ and then dividing by the total degrees of freedom.

For computing orthogonal effects due to the variation in coordinates, we shall approximate $f(x, y)$ by the set of polynomials $P_0, P_1, \ldots$ [20]. The approximation of the piecewise continuous function $f(x, y)$ by the proposed set of orthogonal polynomials can be obtained as follows:

$$f(x, y) \approx \hat{f}(x, y) = \sum_{0 \leqslant j \leqslant t-1} \sum_{0 \leqslant i \leqslant t-1} \beta_{ij} P_i P_j \quad (4)$$

where the expansion coefficients β_{ij} are the desired orthogonal effects. The above equation can be written in matrix notation as follows:

$$[f_{kl}] = \sum_{0 \leqslant i < n} \sum_{0 \leqslant j < n} \beta_{ij} \hat{P}_i \hat{P}_j^t \quad (5)$$

where $\hat{P}_i$ is a column vector of size $(n*1)$ consisting of values of the polynomials $P_i(x)$ at $x = x_1$, $x = x_2, \ldots, x = x_n$, respectively. Let

$$[M] = [\hat{P}_0, \hat{P}_1, \ldots, \hat{P}_{n-1}]$$

Hence

$$[f_{kl}] = [M][\beta_{ij}][M]^t$$

where $[M] \otimes [M]$ is a point spread function as per the classical image formulation model. Since $[M]$ is not unitary, the orthogonal effect can be computed as

$$[\beta_{ij}] = ([M]^t[M])^{-1}([M]^t[f][M])([M]^t[M])^{-1} \quad (6)$$

From Equation 6, the main effects resulting noise, are given by

$$\beta_{ij}^1 = \{\beta_{ij}: 0 < i + j \leqslant 2, i \neq j\} \quad (7)$$

and the interaction effects, characterizing texture, are

$$\beta_{ij}^2 = \{\beta_{ij}: 0 < i, j < 3\} \quad (8)$$

The mean squares corresponding to the orthogonal effects can be computed as

$$[Z_{ij}] = ([M]^t[M])^{-1}([M]^t[f][M])^2 \times ([M]^t[M])^{-1} \quad (9)$$

The following two conjectures were proposed for texture detection.

Texture Conjecture 1 For a textured region, each interaction mean square does not estimate the same variance.

Texture Conjecture 2 For a textured region, mean squares corresponding to some members of the set of main effects may estimate the same variance.

These conjectures are applied to test whether the image region has texture or not.

A small image region $[g]$ of size $(N*N)$ in a digital image is considered as a sample. The two conjectures are applied and the variances are tested with Nair's test [21] given in Appendix A. Finally, the local descriptor of the texture, pronum, is computed as per the algorithm given in Appendix B. Thus we have

$$\begin{bmatrix} g_1 & g_2 & g_3 \\ g_4 & g_5 & g_6 \\ g_7 & g_8 & g_9 \end{bmatrix} \Rightarrow \begin{bmatrix} * & s_1 & s_2 \\ s_3 & s_4 & s_5 \\ s_6 & s_7 & s_8 \end{bmatrix}$$

Gray level image Transformed one

$$\text{pronum} = \sum_{i=1}^{8} s_i * 2^{i-1} \quad (10)$$

and

$$s_i = \{0, 1\}$$

The pronum is substituted in the place of the centre pixel of the $[g]$. In the subsequent phase, adjacent regions are considered by sliding a $(3*3)$ window and the same procedure is repeated. So the entire image is mapped into an array of pronums. The range of pronums considered here is (0–255). The appearance of different pronums and their recurrence reflect the variation of possible combinations of orthogonal effects. So different textured images will have different occurrences of these pronums. The frequency of occurrences of these pronums is used as a global descriptor for the image. The plot showing the variation of the pronums and their frequency of occurrences is called the prospectrum.

3. Experimental procedure

Two sets of photographs (Figs 1a–c and 2a–m) were used for image analysis in this investigation. These photographs were generated as follows [5, 17].

Photographs 1a–c: These were fracture surfaces of tensile specimen observed with the help of a Scanning Electron Microscope (SEM). The dumbell specimens of a natural rubber vulcanizate (Natural rubber, 100, ZnO, 5, Stearic acid 2, Sulphur, 2.5; CBS, 0.8, compound cured for 9 min at 150 °C) with and without precut were tested at 22 °C in a ZWICK machine 1445 (ZWICK GmbH, Germany) according to ASTM D412-80. The chisel cuts of prescribed length were applied through the centre of the test specimen with the help of a special jig. The fracture surfaces were first sputter-coated with gold and then examined under an SEM. Various features of the photographs were investigated at different magnifications.

Photographs 2a–m: These photographs were obtained by Fukahori and Andrews [5]. The test specimens, parallel-sided, (50 mm × 10 mm × 2 mm), containing an edge crack of 1 mm at the centre of the strip were tested at constant crosshead speeds and at temperatures in the range 24–100 °C. The fracture surfaces were metallized by a light-evaporated aluminium coating and examined under an optical microscope. In their analysis, photographic prints of the fracture surfaces were made and lines were drawn at ± 45° to the direction of propagation. The number of intersections per unit length of the lines were counted and each ridge was weighted on an arbitrary four point scale (0.5, 1, 2, 3) according to its depth. The final "Roughness Index" (RI) was obtained by using the weighted total of intersections per length.

3.1. Parameters computed from the images

All the photographs shown in Figs 1 and 2 were digitized in a closed chamber (with uniform illumination) by an electronic scanner (TMC 56 GN-PULNIX CCD camera with 512*512 pixel resolution, focal lengths 16 mm and 8 mm for close and long range, respectively) attached to the Benchmark IPS. The proposed algorithm was used for analysing the images of various fractured surfaces shown in Figs 1 and 2. The prospectrums were obtained and the following parameters were calculated from the prospectrums. The magnification details of Fig. 1 are shown in the photographs. The magnification was 5 × for Fig. 2.

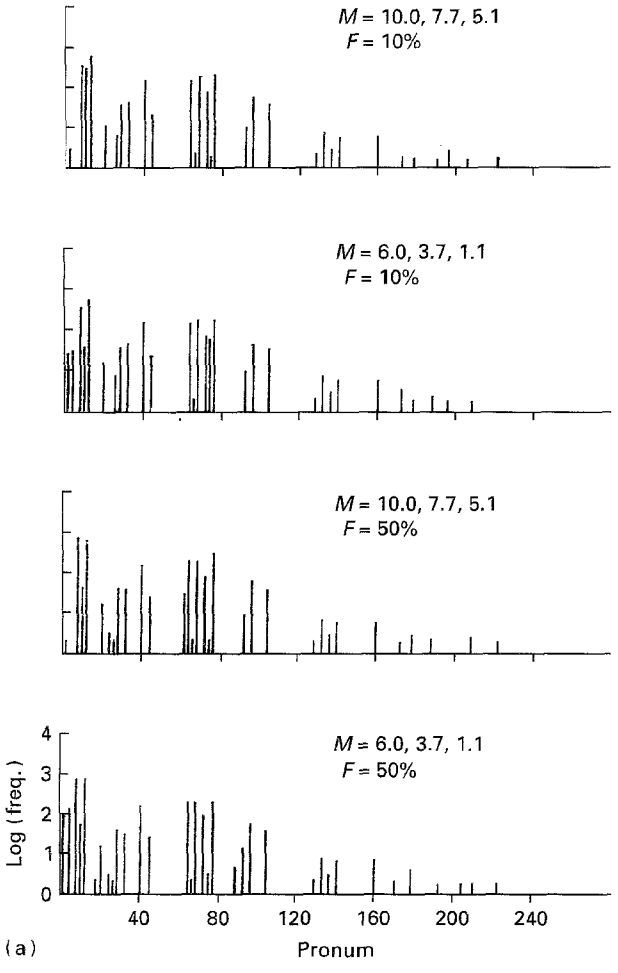

3.1.1. Weighted mean

Representing the "apparent" weighted mean of the prospectrum by μ, the pronum by x_i, the frequency of occurrence of the pronum x_i by the function $F(x_i)$, the "apparent" weighted mean was computed by

$$\mu = \sum_{i=0}^{255} \frac{F(x_i)}{R \times C} \times x_i \qquad (11)$$

where $R*C$ is the total number of pixels in the image. The numbers obtained were converted into "real" quantities by taking into consideration the actual population and its magnification on the photographs.

3.1.2. Variance and standard deviation

The "apparent" variance and the standard deviation for the prospectrums were obtained as follows:

$$\text{variance, } \rho^2 = \sum_{i=0}^{255} (x_i - \mu)^2 \frac{F(x_i)}{R \times C} \qquad (12)$$

and the standard deviation

$$\rho = \sqrt{(\text{variance})}$$

The "real" quantities were also calculated by taking into consideration the actual population and its magnification on the photographs.

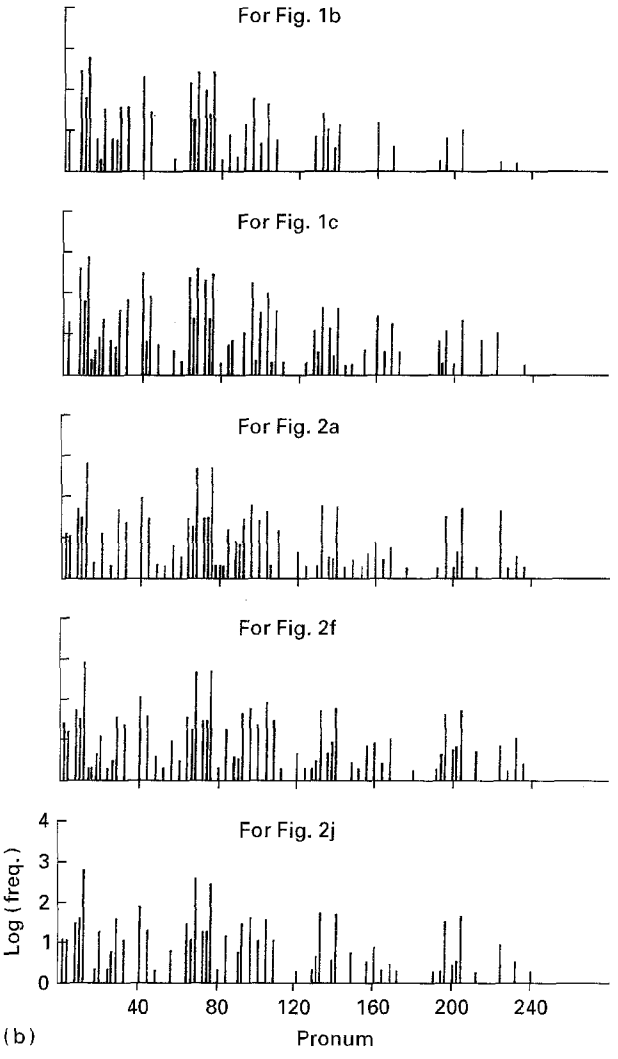

Figure 3 (a) Prospectrums for the image shown in Fig. 1a at different levels of significance. (b) Prospectrums for the images shown in Figs 1b, 1c, 2a, 2f and 2j at M = 10, ... and F = 10% significance.

4. Results and discussion

Photographs 1a–c display the morphology of the fracture surface of the unaged natural rubber samples with different precut lengths. The zone AB represents the precut. In Fig. 1a, fracture initiates at the edges and propagates towards the centre, as the precut length of 0.49 mm is much smaller than the critical cut length. Some tear lines connecting the rough zone and the precut are shown. The fracture surface at the critical cut length (1.21–1.30 mm) is revealed in Fig. 1b. Above the critical value of cut length, fracture starts from the precut and a few tear lines running towards the edges are visible. The three micrographs shown in Fig. 1a–c were quantitatively analysed by digitizing to a gray level variation from 0 to 255. The digitized version of the photographs in Fig. 1a–c is also shown in Fig. 1d–f, respectively. The prospectrum for the image of these micrographs was obtained using the procedure outlined in Appendix B. A representative prospectrum for the sample 1a is shown in Fig. 3a at various significance levels of M and F. The prospectrum has a greater number of components and increase in frequencies, as M and F significance levels are relaxed, i.e. a sample which may not pass the conjecture at the 5% significance level may pass at 10% or higher, leading to an increased frequency of occurrence of the pronum. Other prospectrums in Fig. 3b give similar variation of frequency with pronum for increasing F or M. The results for "real" mean, variance or standard deviation calculated using Equations 11 and 12 are reported in Table I. The "real" quantities are calculated from the "apparent" values by taking the magnification of the photographs into consideration.

Here, the weighted mean of the prospectrum gives an idea about the interspace between the horizontal lines or the tear lines. Similarly, the variance or standard deviation shows the spreading of these pronums in the prospectrum, which is related to the average distance between the tear lines. As F is increased at a constant value of M, the values of mean and variance increase. At a constant value of F, a decrease in M increases these values. The standard deviation also follows a similar trend. The texture plates of all the micrographs 1a–c yield similar information. As the precut length increases, the weighted "real" mean, which indicates the average distance between tear lines, increases. The tensile strength as reported in an earlier paper [17] decreases accordingly. The values of tensile strength at various precut lengths, and the distance between the tear line (D_T) on the photographs taken from [17] are replotted in Fig. 4. The weighted "real" mean value, calculated in this investigation, is plotted against the variation of tensile strength (σ_b) in the same figure. It is evident from the plot that the weighted mean, proportional to the distance between the tear lines and computed by the image processing method, decreases linearly and follows exactly the same trend as the variation of D_T against the tensile strength, σ_b. However, the small difference in their values ($\pm$ 5%) is associated with the method of calculation. The advantage of the image processing technique is to eliminate the laborious procedure involved in earlier measurements.

TABLE I Statistical parameters for Fig. 1

Figure	M	F	"Real" mean	"Real" variance	"Real" std. dev.
1a	10, ...	10%	43	76720	276.9
	8, ...		44	77600	278.6
	6, ...		44	83840	289.5
	10, ...	20%	44	76720	276.9
	8, ...		44	77608	278.6
	6, ...		47	83872	289.6
	10, ...	50%	46	78240	279.7
	8, ...		46	79440	281.8
	6, ...		59	108676	329.6
1b	10, ...	10%	106	155500	394.3
	8, ...		106	156480	395.5
	6, ...		107	156704	395.9
	10, ...	20%	106	155528	394.4
	8, ...		106	156832	396.0
	6, ...		107	158672	398.3
	10, ...	50%	106	155812	394.7
	8, ...		108	159124	398.9
	6, ...		117	163424	404.3
1c	10, ...	10%	254	285712	534.5
	8, ...		255	286452	535.2
	6, ...		255	286592	535.3
	10, ...	20%	254	285844	534.6
	8, ...		255	287296	536.0
	6, ...		256	288650	537.3
	10, ...	50%	256	287552	536.2
	8, ...		258	288856	537.5
	6, ...		262	299712	545.6

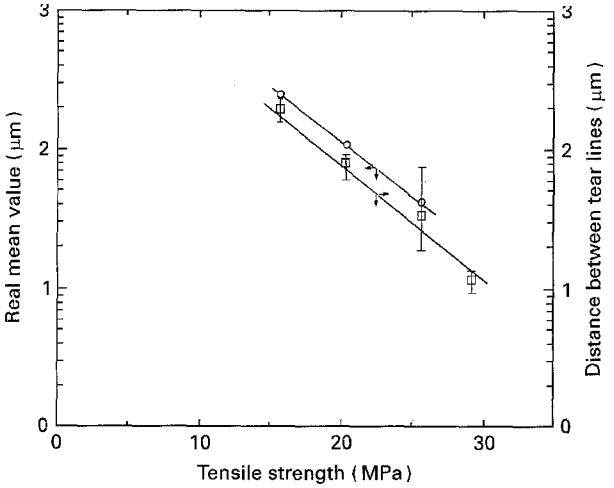

Figure 4 Plot of distance between the tear lines (D_T) measured manually and computed in terms of the "real" mean by the proposed method versus tensile strength (σ_b) (○) Present work; (□) Deuri and Bhowmick [17].

In the earlier photomicrographs, there is a regular pattern. However, such regularity is not observed on the other fracture surfaces such as those reported by Fukahori and Andrews [5]. The torn fractured surfaces are shown in Fig. 2a–m. It is visually apparent that the surface roughness varies with the strain rate and temperature. For SBR, the roughness decreases with the strain rate. The digitized version of the photographs is also shown in Fig. 2a–m. These images were also analysed as per the procedure discussed earlier in this paper and their prospectrums obtained. Fig. 3b shows the representative prospectrums for the images shown in Fig. 2a, f and j. As expected, the prospectrum has a greater number of components and increase in frequencies, as M and F significant levels are relaxed.

TABLE II Statistical parameters for Fig. 2

Figure	"Real" mean (μm)	Roughness quantity (μm^{-1})
2a	2280	439
2b	2680	373
2c	2980	336
2d	3540	283
2e	3760	266
2f	2740	365
2g	2800	357
2h	2940	340
2i	3340	299
2j	1980	505
2k	2040	490
2l	2120	471
2m	2380	420

Significance level M = 10, ... and F = 10%

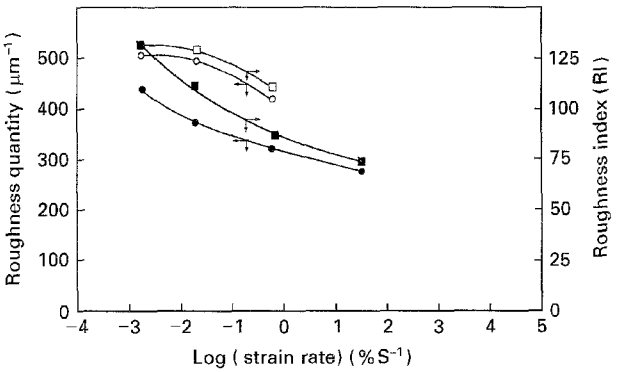

Figure 5 Plots of the "roughness quantity" and "roughness index" as a function of strain rate for the images shown in Fig. 2. (□) 100 °C, Fukahori and Andrews [5]; (○) 100 °C, present work; (■) 24 °C, Fukahori and Andrews [5]; (●) 24 °C, present work.

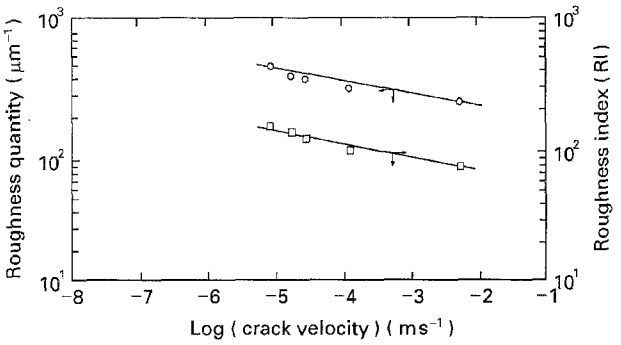

Figure 6 Plots of "roughness quantity" and "roughness index" versus crack velocity for Fig. 2a–e. (○) Present work; (□) Fukahori and Andrews [5].

The weighted mean is computed from the prospectrums and the "roughness quantity" which has been taken as inverse of the weighted real mean has been computed. Conceptually, the weighted "real" mean is inversely proportional to the "roughness index" discussed in the paper by Fukahori and Andrews [5]. This is for the following reason: In the "tolysurf" method, a very light step is assigned an arbitrary value of 0.5. Hence a surface having more such light steps will have a low roughness index, although the surface is more textured, giving a higher mean value. Similarly, a heavy step is assigned a weight of 3.0. Even a few such steps will give rise to larger "roughness index", whereas the same surface will have less textured information, and hence a lower mean. Various statistical parameters and the "roughness quantity"

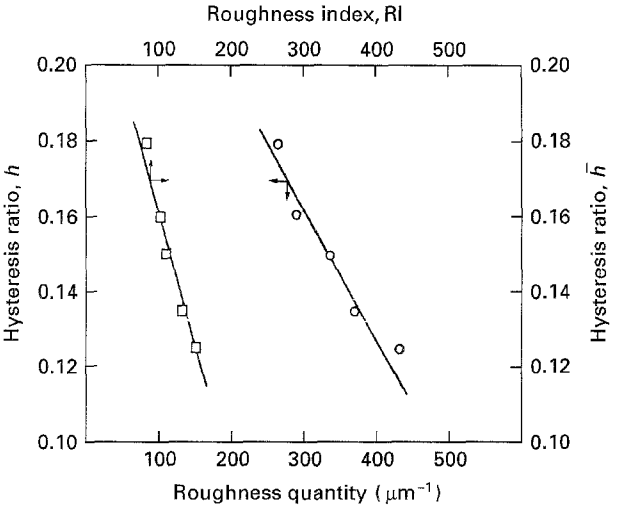

Figure 7 Plots of hysteresis ratio ($\bar{h}$) versus "roughness quantity" and "roughness index" for Fig. 2a–e. (○) Present work; (□) Fukahori and Andrews [5].

computed from the real mean are reported in Table II. The data for the roughness index at various strain rates and crack velocities, hysteresis ratio of samples tested at different strain rates and temperatures were collected from [5]. Figs 5, 6 and 7 are drawn by taking the "roughness quantity" (RQ) computed from the weighted mean with various other earlier parameters – crack velocity ($\dot{c}$), strain rate ($\dot{\varepsilon}$) and hysteresis ratio ($\bar{h}$). These were then compared with the trend in Fukahori and Andrew's paper [5]. It is interesting to note that in Figs 5 and 6, the trend in results is similar. For example, "roughness quantity" is linearly proportional to the crack velocity and the gradient of the lines (our work and earlier work) is the same. However the plot of the hysteresis ratio against the "roughness quantity" shows some difference. This is because the roughness index calculated earlier was obtained by using the "tolysurf" method which has used "arbitrary" numbers for the description of the intensity of the point. But the present method is computerized and fast, requiring no human intervention.

The straight lines shown in Figs 4, 6 and 7 for the present work could be described by the following empirical relationships, respectively:

$$\log(D_T) = 3.6 - 0.075\sigma_b \quad (13)$$

$$\log(RQ) = 2.185 + 0.095\log(\dot{c}) \quad (14)$$

$$\bar{h} = 0.2646 - 3.59 \times 10^{-4}(RQ) \quad (15)$$

Equation 13 is the same as that derived manually by Deuri and Bhowmick [17].

5. Conclusions

The statistical design of this experiments' approach has been effectively used for quantification of the roughness of fractured rubber surfaces. The "textured" surfaces have been represented in terms of a closed set of orthogonal polynomials and the variation due to the cartesian coordinates has been measured in terms of main and interaction effects. The main effects are those in which one coordinate is varying while the other remains constant, whereas the interaction effects are the effects due to the variation of both coordinates. Conjectures have been proposed for quantifying the

texture present. In tensile fractured surfaces of NR vulcanizate with a precut, the statistical "real" weighted mean computed from the prospectrum is proportional to the distance between the tear lines. The results are in good accord with those published earlier. Further, this method has also been applied for quantitative analysis of fractured surfaces obtained by Fukahori and Andrews [5]. The weighted real mean computed from the prospectrum is inversely proportional to the roughness index. The "roughness quantity" computed from the mean has been plotted against the variation of crack velocity, strain rate and hysteresis ratio as done in their work. A similar trend between various parameters has been obtained. Using the image processing technique proposed, a large amount of laborious procedure in quantification can be easily avoided.

Appendix 1. Nair's criterion

Nair's test for checking the Homogeneity of variances is given below.

Let $v_{a_1}, v_{a_2}, \ldots, v_{a_k}$ be the set of variances with $\upsilon_1, \upsilon_2, \ldots, \upsilon_k$ degrees of freedom, respectively.

The average variance

$$v_{av} = \frac{1}{\upsilon} \sum_{i=1}^{k} v_{a_i} \upsilon_i$$

and the total degrees of freedom

$$\upsilon = \sum_{i=1}^{k} \upsilon_i$$

then the criterion for computing the divergence among variances is

$$M_1 = \upsilon \ln v_{av} - \sum_{i=1}^{k} \upsilon_i \ln(v_{a_i})$$

The values of M_1 for different degrees of freedom and for different percentage significance levels are given in [21].

Appendix 2. Algorithm

Input Gray level image G of size ROW*COL. [ ] denotes the matrix and the suffix denotes the elements of the matrix. Let $[M]$ be the polynomial operator and $[f]$ be a (3*3) image region extracted from G. PROARR holds the pronums obtained from G.

Output Prospectrum, i.e. frequency of occurrences of pronums (at most 256 different pronums may appear).

Begin

Step 1 Compute $[W] = [M]^t[M]$ where

$$[M] = \begin{bmatrix} 1 & -1 & 1 \\ 1 & 0 & -2 \\ 1 & 1 & 1 \end{bmatrix}$$

Step 2 Repeat thru step 15 for $k = 2$ to ROW-1

Step 3 Repeat thru step 14 for $1 = 2$ to COL-1

Step 4 Extract a small region $[f]$ from G centred at $(k, 1)$

Step 5 Compute $[\beta'] = [M]^t[f][M]$

Step 6 Compute

$[\beta] = ([M]^t[M])^{-1}([M]^t[f][M])$

$([M]^t[M])^{-1} = [\beta']/([W]_{i,i} * [W]_{j,j})$

Step 7 Compute $[Z] = ([\beta']_{i,j})^2/([W]_{i,i} * [W]_{j,j})$

Step 8 $A = \{Z_{01}, Z_{02}, Z_{10}, Z_{20}\}$ are variances due to the main effects and $B = \{Z_{11}, Z_{12}, Z_{21}, Z_{22}\}$ are variances due to the interaction effects.

Step 9 Perform Nair's test for sets A and B. If the test fails, pronum $= -1$, indicating there is no texture. Go to step 14. (While performing Nair's test, if all four variances do not pass the test, then eliminate one variance at a time and perform the test again. In the worst case, there must be two variances present.)

Step 10 Let set $V \subseteq A$ have variance terms that pass Nair's Test and $\| V \|$ be the cardinality of set V.

Step 11 Compute the mean square error variance, msv $= (\sum_{Z_{ij} \in V} Z_{ij})/\| V \|$.

Step 12 Perform the variance ratio test [22] (F ratio test), with numerator as one of the variances from $\{A + B - V\}$ and msv as the denominator, against the chosen significance level. If the test is significant, the corresponding position p_i of the numerator in the image region $[f]$ is marked as 1, otherwise as 0.

Step 13 Compute the pronum for the image region $[f]$ as: pronum $= \sum_{i=1}^{8} p_i * 2^{i-1}$, $p_i = 1$ if the ith position is 1; otherwise 0.

Step 14 Store the pronum in PROARR$[k][l]$ and increment l by 1.

Step 15 Increment k by 1.

Step 16 Compute the frequency of occurrences of pronums from PROARR.

End

References

1. A. G. THOMAS and H. W. GREENSMITH, *J. Polym. Sci.* **18** (1955) 189.
2. A. G. THOMAS, *J. Appl. Polym. Sci.* **3** (1960) 168.
3. H. W. GREENSMITH, *ibid.* **3** (1960) 83.
4. A. K. BHOWMICK, *Kautschuk und Gummi Kunststoffe* **37** (1984) 191.
5. Y. FUKAHORI and E. H. ANDREWS, *J. Mater. Sci.* **13** (1978) 777.
6. A. SCHALLAMACH, *Rubber Chem. Technol.* **41** (1968) 209.
7. *Idem., Wear* **1** (1958) 384.
8. A. K. BHOWMICK, *Rubber Chem. Techol.* **55** (1982) 1055.
9. A. K. BHOWMICK, S. BASU and S. K. DE, *ibid.* **53** (1980) 321.
10. A. K. BHOWMICK, *J. Mater. Sci. Lett.* **5** (1986) 1042.
11. N. ROYCHOWDHURY and A. K. BHOWMICK, *J. Mater. Sci.* **25** (1990) 2985.
12. A. SAHADEURI and A. K. BHOWMICK, *J. Appl. Polym. Sci.* **35** (1988) 327.
13. A. GOLDBERG, D. R. LESEUR and J. PATT, *Rubber Chem. Technol.* **62** (1989) 272.
14. A. I. MEDALIA, A. L. ALESI, J. L. MEAD and R. SIMONEAU, *ibid.* **62** (1989) 165.
15. A. K. BHOWMICK and S. K. DE (eds), "Fractography of Rubbery Materials" (Elsevier Applied Science, London, 1991).
16. A. N. GENT and C. T. R. PULFORD, *J. Mater. Sci.* **19** (1984) 3612.
17. A. S. DEURI and A. K. BHOWMICK, *ibid.* **22** (1987) 4299.
18. P. THAVAMANI and A. K. BHOWMICK, *Rubber Chem. Technol.* **67** (1994) 129.
19. P. BHATTACHARYYA, PhD thesis, Dept. of Computer Science and Engineering, Indian Institute of Technology, Kharagpur (1984).
20. L. GANESAN and P. BHATTACHARYYA, Statistical design of experiments approach for texture description, pattern recognition, in press.
21. D. J. BISHOP and U. S. NAIR, *Biometrika* **89–99** (1939).
22. R. A. FISHER and F. YATES, *Statistical Tables for Biological, Agricultural and Medical Research* (Oliver and Boyd, London, 1947).

Received 22 December 1994
and accepted 7 June 1995